Ecological Risk and Security Research (2024) Volume 2 Issue 2
doi: 10.59429/ersr.v2i2.10985

RESEARCH ARTICLE

Utilization of citric acid-modified chitosan derived from oyster shells for the adsorptive removal of cadmium ions from wastewater

Akanbi, Magdalene Nkeiru [1*]; Ejidike, Lynda Chinyere [2]; Eze, Patricia Nnebuogo [3]; Okore, Glory Jerry [4]; Aharanwa, Bibiana Chimezie [5]; Oze, Nwanneamaka Rita [6]

[1*] *Department of Polymer Engineering, Federal University of Technology Owerri, Nigeria magakanbi2009@gmail.com (Corresponding Author)*

[2] *Department of Chemistry, Nnamdi Azikiwe University, Awka, Nigeria lindaejidike@gmail.com*

[3] *Department of Chemistry, Federal College of Education (Technical) Asaba, Nigeria patricia.eze@fcetasaba-edu.ng*

[4] *Department of chemistry, Alvan Ikoku Federal University of Education, Owerri, Nigeria gloryokore150@gmail.com*

[5] *Department of Polymer Engineering, Federal University of Technology, Owerri, Nigeria bibyahas@gmail.com*

[6] *Department of Chemistry, Federal University of Technology, Owerri, Nigeria nwanneamaka.oze@futo.edu.ng*

*** Corresponding author:** AKANBI Magdalene Nkeiru, magakanbi2009@gmail.com

ABSTRACT

The increasing contamination of water bodies by heavy metals, particularly cadmium (Cd^{2+}), poses a significant threat to environmental and public health due to its toxicity, persistence, and bioaccumulate nature. This study investigates the potential of citric acid-modified chitosan, derived from oyster shells, as an eco-friendly and cost-effective adsorbent for the removal of cadmium ions from aqueous solutions. Chitosan was extracted through deproteination, demineralization, and deacetylation processes, followed by chemical modification using citric acid to enhance its adsorption properties. Characterization of the modified chitosan was conducted using Fourier Transform Infrared Spectroscopy (FTIR), UV–Visible Spectroscopy (UV–Vis), and Atomic Absorption Spectrophotometry (AAS). FTIR analysis confirmed the successful transformation of oyster shell into chitosan, with the emergence of functional groups such as hydroxyl, carbonyl, and amine groups critical for metal ion binding. UV–Vis. spectroscopy revealed strong absorbance in the UV region and optical transparency in the visible range, indicating high purity and suitability for biomedical and environmental applications. Batch adsorption experiments were performed to evaluate the effects of initial cadmium concentration, contact time, and temperature. The results showed that maximum adsorption occurred at low concentrations, with equilibrium reached at 60 minutes and optimal performance at 40°C. Isotherm modeling revealed that the Freundlich model ($R^2 = 0.8389$) better described the adsorption behavior than the Langmuir model (R^2

ARTICLE INFO
Received: 12 August 2024 | Accepted: 7 October 2024 | Available online: 11 December 2024

CITATION
A.M.N. Akanbi, L.C. Ejidike, P.N. Eze, G.J. Okore, B.C. Aharanwa, N.R. Oze。Utilization of citric acid modified chitosan derived from oyster shells for the adsorptive removal of cadmium ions from wastewater. *Ecological Risk and Security Research* 2024; 2(2): 10985.doi: 10.59429/ersr.v2i2.10985

= 0.0245), suggesting multilayer adsorption on a heterogeneous surface. Kinetic studies indicated that the pseudo-second-order model (R^2 = 0.9738) best fit the data, implying chemisorption as the dominant mechanism. Overall, the study demonstrates that citric acid-modified chitosan is a promising biosorbent for cadmium removal, offering a sustainable solution for wastewater treatment. Further optimization and real-world application studies are recommended to enhance its practical viability.

Keywords: Wastewater treatment; adsorption studies; kinetics; crustaceans shells; cadmium metal

1. Introduction

Heavy metal contamination in aquatic environments has become a pressing global concern due to its persistence, toxicity, and increasing bioaccumulation levels in nature. Among these pollutants, cadmium (Cd^{2+}) is particularly notorious due to its high toxicity, non-biodegradability, and tendency to bioaccumulate in living organisms. Cadmium exposure, even at low concentrations, has been linked to severe health conditions such as kidney damage, renal dysfunction, bone demineralization, and carcinogenic effects [1]. Its primary sources include industrial discharges from battery manufacturing, electroplating, pigment production, and mining operations [2,3].

Traditional methods for cadmium removal, such as chemical precipitation, ion exchange, and membrane filtration, are often limited by high operational costs, sludge generation, and inefficiency at low metal concentrations [4]. Also, the generation of secondary pollutants is highly probable, making them less sustainable for long-term environmental management. The success of adsorption largely depends on the choice of adsorbent, and in recent years, biopolymers like chitosan derived from chitin have gained significant attention for its high affinity toward heavy metal ions, owing to its amino and hydroxyl functional groups [5].

Recent studies have explored the modification of chitosan to enhance its adsorption capacity and selectivity. Gamage et al. [6] reviewed the application of chitosan-based composites and nanocomposites, highlighting their improved physicochemical properties and performance in removing metals like cadmium, lead, and chromium from contaminated water. These modifications often involve cross-linking with organic acids, incorporation of nanoparticles, or blending with other biopolymers to increase surface area and binding sites. Wang et al. [7] developed chitosan-based carbon nanoparticles (chi-CNPs) that not only removed heavy metals efficiently but also served as fluorescent indicators for metal ion detection. Their study demonstrated a cadmium removal efficiency of over 54%, significantly outperforming conventional carbon-based adsorbents. Similarly, a systematic review by Tsauria et al. [8] emphasized the role of functionalized chitosan in improving adsorption kinetics, regeneration potential, and adaptability for industrial-scale wastewater treatment. Despite these advancements, challenges remain. Many studies are conducted under controlled laboratory conditions using synthetic wastewater, which may not accurately reflect the complexity of real industrial effluents. Additionally, the regeneration and reuse of chitosan-based adsorbents, while promising, require further optimization to ensure economic viability and environmental sustainability.

Chitosan, derived from the deacetylation of chitin found in crustacean shells, is a biodegradable, non-toxic, and renewable material with excellent metal-binding properties [9]. However, raw chitosan has limitations in terms of mechanical strength, solubility, and adsorption capacity. To overcome these drawbacks, chemical modifications such as cross-linking or functionalization with organic acids have been employed to enhance its performance [10]. Although chitosan has demonstrated significant potential as an eco-friendly adsorbent for heavy metal removal, its practical application in real-world wastewater treatment

systems remains limited. Most existing studies focus on synthetic solutions and do not account for the complex matrix of industrial effluents, which may contain competing ions and organic matter that affect adsorption efficiency [6]. Furthermore, while chemical modifications such as citric acid activation have been shown to enhance chitosan's performance, there is a lack of standardized protocols for optimizing these modifications across different wastewater conditions [7]. The scalability, cost-effectiveness, and long-term stability of modified chitosan also remain underexplored. Therefore, there is a critical need for comprehensive studies that bridge the gap between laboratory research and field application, particularly in developing regions where affordable and sustainable water treatment solutions are urgently required.

This study explores the use of citric acid-modified chitosan, extracted from oyster shells, as a sustainable and efficient adsorbent for the removal of cadmium ions from synthetic wastewater. The modification process aims to increase the number of active binding sites and improve the structural integrity of the chitosan matrix. The research is grounded in the broader context of circular economy and waste valorization, as it transforms seafood waste into a valuable material for environmental remediation [11,12]. The study aims to evaluate the effectiveness of citric acid-modified chitosan in adsorbing cadmium ions from synthetic wastewater under varying conditions: temperature, contact time, and initial metal concentration. The objective seeks to characterize the modified chitosan using analytical techniques such as FTIR, UV-Vis. spectroscopy, and AAS, and to model the adsorption process using kinetic and isotherm equations to better understand the underlying mechanisms. Ultimately, the study explores the potential of modified chitosan as a low-cost, eco-friendly solution for cadmium removal in wastewater treatment applications. By addressing these objectives, this research contributes to the growing body of knowledge on biopolymer-based adsorbents and offers a sustainable pathway for mitigating heavy metal pollution in water systems

2. Materials and methods

2.1. Preparation of adsorbent

Chitosan was extracted from oyster shells through a multi-step process involving deproteination, demineralization, and deacetylation (Figure 1). The shells were first washed, sun-dried, pulverized, and sieved (300μm mesh) to a fine powder. Deproteination was carried out using 1 M NaOH on 150g of fine powder at 90°C for 1 hour, followed by demineralization with 1 M HCl under continuous stirring. The resulting chitin was then deacetylated using 0.5 M NaOH at 50°C for 12 hours to yield chitosan [13]. To enhance its adsorption capacity, 80g of chitosan was modified by treating it with 0.25 M citric acid at 60°C for 1 hour under magnetic stirring. The modified chitosan was rinsed with distilled water and air-dried at room temperature [12,14].

2.2. Preparation of adsorbate

Aqueous cadmium ion solutions were prepared by dissolving cadmium nitrate in distilled water to obtain concentrations ranging from 2, 3, 5 and 10 ppm. The pH of the solutions was adjusted to pH 5.0 using dilute HCl or NaOH, as required.

2.3. Characterization

To evaluate the structural, chemical, and functional properties of the modified chitosan used for cadmium ion adsorption, three key analytical techniques were employed; Fourier Transform Infrared Spectroscopy (FTIR), Atomic Absorption Spectrophotometry (AAS), and UV–Visible Spectroscopy (UV–Vis). Each technique was selected for its ability to provide specific insights into the material's composition and performance [15].

2.3.1. Fourier Transform Infrared Spectroscopy (FTIR)

FTIR analysis was conducted to identify the functional groups present in both the pulverized oyster shell and the extracted chitosan. The spectra were recorded in the range of 4000–400 cm^{-1} using a calibrated FTIR spectrometer. Before analysis, the instrument was baseline-corrected using a clean KBr pellet as a reference. The samples were prepared by mixing with KBr and pressing into pellets. In the Quality assurance and control (QA/C), where spectral resolution was maintained at 4 cm^{-1}, each sample was scanned three times to ensure reproducibility, and the background scans were performed before each sample run [16].

2.3.2. Atomic Absorption Spectrophotometry (AAS)

AAS was used to quantify cadmium ion concentrations in solution before and after adsorption. The analysis was performed using a flame AAS equipped with a cadmium hollow cathode lamp, operated at a wavelength of 228.8 nm. Calibration was performed using standard cadmium solutions (0.5, 1.0, 2.0, 5.0, and 10.0 ppm) prepared from certified reference materials. The instrument was zeroed with deionized water, and a calibration curve was generated with an R^2 value above 0.995 to ensure linearity. Sample solutions were filtered and acidified with HNO_3 before analysis to prevent precipitation and matrix interference [17]. The QA/C measures were that calibration standards were run before and after every 10 samples, a blank and a quality control check standard were analyzed every 5 samples, and all glassware was acid-washed and rinsed with deionized water.

2.3.3. UV–Visible Spectroscopy (UV–Vis)

UV–Vis. spectroscopy was employed to assess the purity and structural integrity of the extracted chitosan. The absorbance spectrum was recorded from 200 to 700 nm using a double-beam UV–Vis spectrophotometer. The chitosan sample exhibited a strong absorbance peak between 200–230 nm, attributed to π–π^* transitions of chromophores such as carbonyl groups. The absence of significant absorbance beyond 300 nm confirmed the optical clarity and low impurity content of the sample. The QA/C measures were that the spectrophotometer was calibrated using a quartz cuvette and baseline-corrected with distilled water, all measurements were performed in triplicate and the instrument was validated using a potassium dichromate standard solution [17-19].

2.4. Experimental studies

Batch adsorption experiments were conducted to evaluate the effects of Initial metal ion concentration, Contact time and temperature [20-22]. All experiments were conducted in triplicate to ensure reproducibility.

2.4.1. Initial metal concentrations

100 mL of cadmium solutions at varying concentrations (2 ppm, 3 ppm, 5 ppm and 10 ppm) were treated with 0.5 g of modified chitosan. After 60 minutes of agitation at 40°C, the residual cadmium solutions were filtered and analyzed using AAS.

The absorption efficiency (%) was calculated as

$$Absorption\ capacity\ (\%) = \frac{C_0 - C_e}{C_0} \times 100 \quad (1)$$

Where:

Co is the initial concentration (ppm)

Ce is the equilibrium concentration (ppm)

2.4.2. Effect of contact time

0.5 g of adsorbent was added to 100 mL of 5.32 ppm cadmium solution. Samples were withdrawn at intervals (20 to 60 min), filtered, and analyzed using AAS. The absorption capacity at time, t:

$$Absorption\ capacity\ (q_t) = \frac{C_0 - C_t}{m} \times V \quad (2)$$

Where:

q_t is the absorption capacity at time t (mg/g)

C_t is the concentration at time t (ppm)

V is the volume of solution (L)

m is the mass of absorbent (g)

2.4.3. Effect of temperature

For the effect of temperature, 0.5 g of adsorbent was added to 100 mL of 10 ppm cadmium solution and agitated at 40°C, 60°C, 80°C, and 100°C for 60 minutes. The residual concentration was measured. The mixtures were agitated in a water bath and filtered after equilibrium. Residual cadmium concentrations were measured using Atomic Absorption Spectrophotometry (AAS).

2.5. Adsorption studies

Equilibrium data were analyzed using both Langmuir and Freundlich models, as they helped determine the adsorption capacity and surface characteristics of the modified chitosan [23,24].

Langmuir isotherm model, which assumes monolayer adsorption on a homogeneous surface. The formula is

$$Linear\ Form: \left(\frac{1}{q_e}\right) = \left(\frac{1}{q_{max} K_L C_e}\right) + \left(\frac{1}{q_{max}}\right) \quad (3)$$

Where:

q_e is the amount adsorbed at equilibrium (mg/g)

q_{max} is the maximum adsorption capacity (mg/g)

K_L is the Langmuir constant (L/mg)

Freundlich isotherm model, which accounts for heterogeneous surface energies and multilayer adsorption

$$Linear\ Form: \log q_e = \log K_F + \frac{1}{n} \log C_e \quad (4)$$

Where:

K_F is Freundlich constant (mg/g) $(L/mg)^{(1/n)}$

n is the adsorption intensity

2.6. Kinetic studies

The adsorption kinetics were evaluated using Pseudo First and second order models. The kinetic parameters were derived from linear plots of the respective models, and the best-fitting model was determined based on correlation coefficients [8,25].

Pseudo-first-order model, which assumes the rate of occupation of adsorption sites is proportional to the number of unoccupied sites

$$\log(q_e - q_t) = \log q_e - \frac{k_1}{2.303} t \quad (5)$$

Where:

q_e is the amount adsorbed at equilibrium (mg/g)

q_t is the amount adsorbed at time, t (mg/g)

k_1 is rate constant (1/min)

Pseudo-second-order model, which assumes chemisorption as the rate-limiting step

$$\frac{t}{q_t} = \frac{1}{k_2 q_e^2} + \frac{t}{q_e} \quad (6)$$

Where:

K_2 is the rate constant of second order adsorption (g/mg.min)

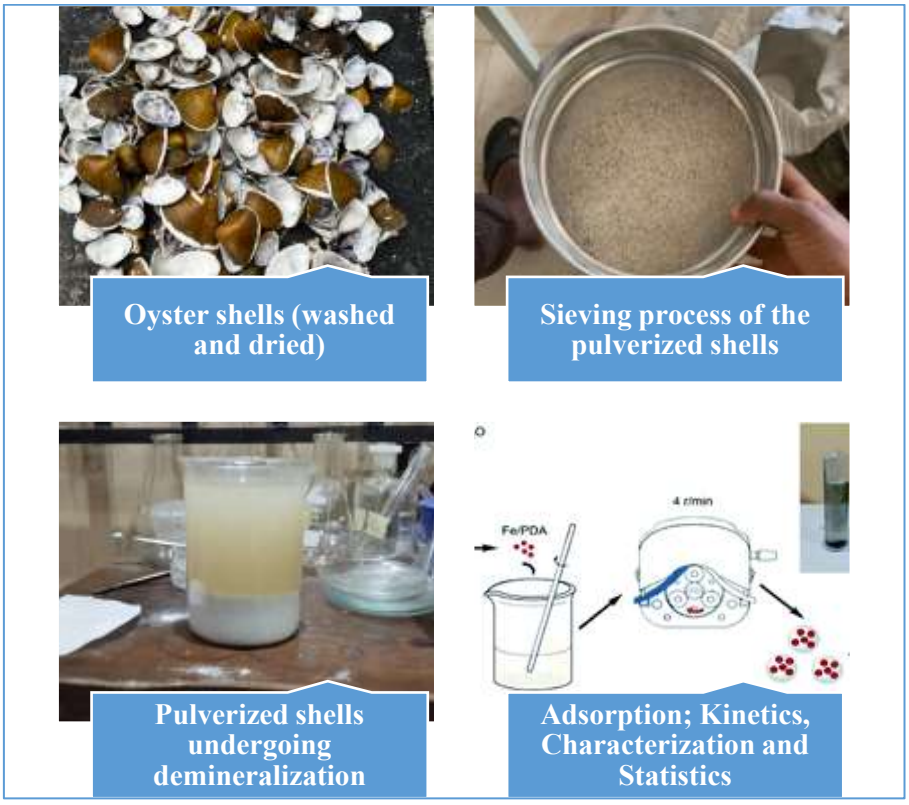

Figure 1. Methodology Flow Process

2.7. Statistical Analysis

Experimental data were analyzed using regression analysis to determine the best-fitting kinetic and isotherm models. Regression analysis was performed using Microsoft Excel. Model accuracy was assessed using correlation coefficients (R^2), and residual plots were examined to evaluate goodness-of-fit.

3. Results and discussion

3.1. Characterization

3.1.1. FTIr characterization of pulverized shells and extracted chitosan

FTIR spectroscopy was employed to identify the functional groups present in both the pulverized oyster shell and the extracted chitosan. The spectra data provide insight into the chemical transformations that occurred during the extraction and modification processes. The FTIR spectrum of the pulverized oyster shell revealed several characteristic peaks (Figure 2 and Table 1). A broad peak at 3360 cm^{-1} corresponds to O–H stretching, indicating the presence of hydroxyl groups, which are commonly found in alcohols, phenols, or carboxylic acids. The peak at 3020 cm^{-1} is attributed to =C–H stretching, suggesting the presence of aromatic or alkene compounds. A distinct peak at 1637 cm^{-1} corresponds to C=O stretching, which is indicative of carbonyl or carboxyl groups, possibly from proteins or organic acids. The peak at 1238 cm^{-1} is associated with C–N stretching, pointing to the presence of amines or amide functionalities. Additional peaks at 2047 cm^{-1} (C≡C) and 2244 cm^{-1} (C≡N) suggest the presence of alkyne and nitrile groups, which may be due to impurities or trace organic compounds. The presence of S–H stretching at 2540 cm^{-1} and aldehyde C–H stretching at 2744 cm^{-1} further supports the complex organic composition of the raw shell material. These findings confirm that the pulverized oyster shell contains a variety of organic and inorganic functional groups, including hydroxyl, carbonyl, amine, and aromatic structures, which are typical of biological calcium carbonate matrices [26,27].

The FTIR spectrum of the extracted chitosan showed significant changes, indicating successful deacetylation and modification (Figure 3 and Table 2). A broad and intense peak at 3417 cm^{-1}, along with a secondary peak at 3602 cm^{-1}, corresponds to O–H stretching vibrations, confirming the presence of hydroxyl groups. The peak at 1748 cm^{-1} is due to C=O stretching, suggesting the presence of carbonyl groups, likely from residual acetyl groups or ester linkages introduced during citric acid modification. A strong peak at 1166 cm^{-1} is attributed to C–O stretching, indicating the presence of alcohols, ethers, or esters. Peaks at 2852 cm^{-1} and 2924 cm^{-1} correspond to C–H stretching in alkanes, confirming the presence of aliphatic hydrocarbon chains. Additional peaks at 1427 cm^{-1} (O–H bending) and 1626 cm^{-1} (C=C stretching) suggest the presence of phenolic and aromatic structures, possibly from residual organic matter or modification agents [16].

These spectral features are consistent with those reported in the literature for chitosan and its derivatives. The presence of hydroxyl, carbonyl, and amine groups confirms the successful extraction and chemical modification of chitosan from oyster shells. The similarity of these peaks to those reported by Sumaila et al. [20] and Lalit Mahatma [28] further validates the identity and purity of the extracted chitosan.

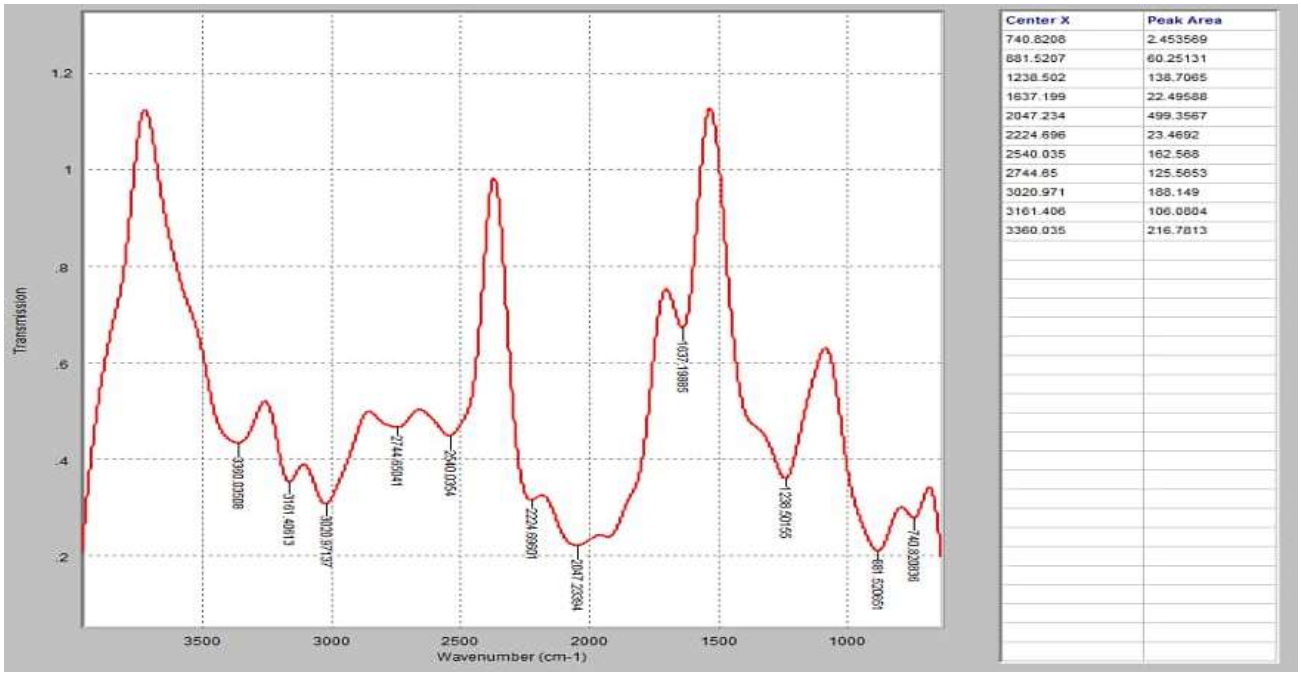

Figure 2. FTIR analysis of pulverized shell

Table 1. FTIR analysis of pulverized oyster shell

Wave Number (cm^{-1})	Peak Area	Bond	Vibration Mode	Functional Group Classification
740.82	2.45	C–H	Out-of-plane bending	Aromatic groups
881.52	60.25	C–H	Out-of-plane deformation	Aromatic compounds
1238.50	138.71	C–N	Stretching	Amines or Amides
1637.20	22.46	C=O	Stretching	Carbonyl or Carboxyl groups
2047.23	499.36	C≡C	Stretching	Possible impurities
2244.90	23.47	C≡N	Stretching	Nitrile functional groups
2540.04	162.57	S–H	Stretching	Thiol groups
2744.85	125.57	C–H	Stretching	Aldehyde groups
3020.97	148.15	=C–H	Stretching	Alkenes or Aromatic compounds
3161.41	106.09	N–H	Stretching	Amines or Amides
3360.04	216.78	O–H	Stretching	Hydroxyl groups

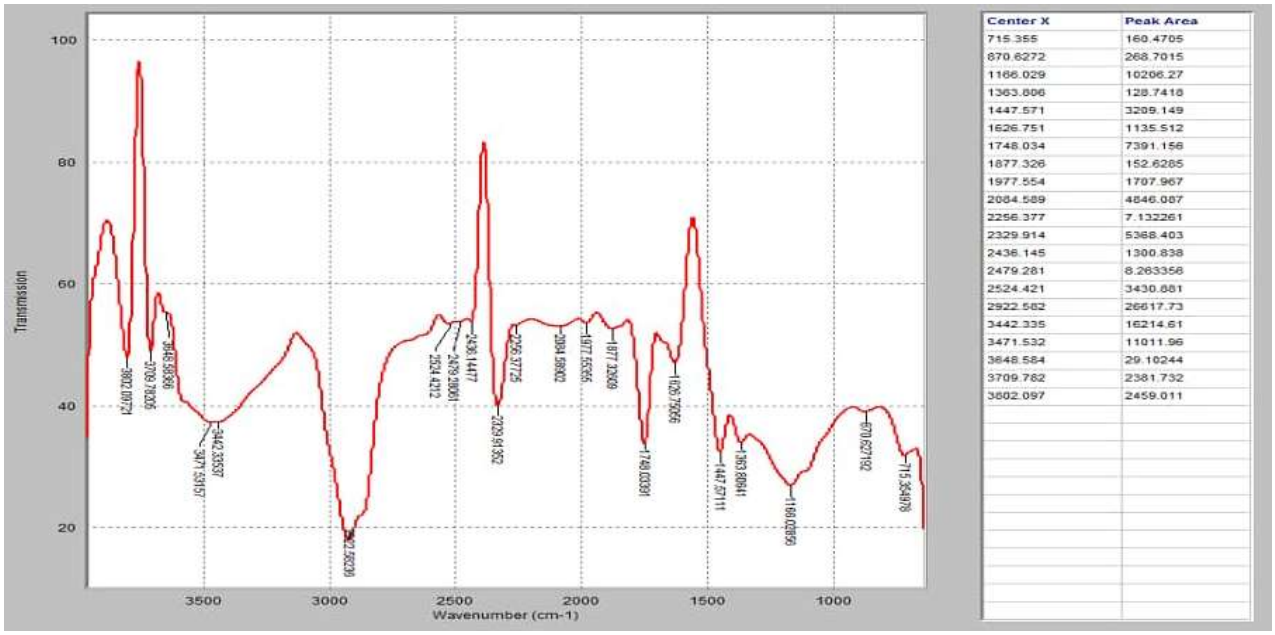

Center X	Peak Area
715.355	160.4705
870.6272	268.7015
1166.029	10206.27
1363.696	128.7418
1447.571	3209.149
1626.751	1135.512
1748.034	7391.156
1877.326	152.6285
1977.554	1707.967
2084.589	4646.087
2256.377	7.132261
2329.914	5368.403
2436.145	1300.838
2479.281	8.263356
2524.421	3430.881
2922.582	26617.73
3442.335	16214.61
3471.532	11011.96
3648.584	29.10244
3709.782	2381.732
3602.097	2459.011

Figure 3. FTIR analysis for the extracted chitosan sample

Table 2. FTIR analysis of extracted chitosan sample

Wave Number (cm^{-1})	Peak Area	Bond	Vibration Mode	Functional Group Classification
715.36	160.47	C–H	Out-of-plane bending	Aromatic rings
870.63	268.70	C–H	Out-of-plane deformation	Aromatic or Vinyl groups
1166.03	10206.27	C–O	Stretching	Alcohols, Ethers, or Esters
1363.01	128.74	C–H	Bending	Alkanes
1427.57	3209.15	O–H	Bending	Phenolic group
1626.15	1135.51	C=C	Stretching	Alkenes or Aromatic rings
1748.03	7391.16	C=O	Stretching	Carbonyl groups in Esters or Ketones
1977.55	1707.97	–	–	Overtone or combination bands
2084.59	522.62	C≡N	Stretching	Nitrile groups
2332.91	5386.40	CO_2	–	Nitrile groups
2489.28	8.26	–	–	Rarely seen functional groups.
2852.54	2617.17	C–H	Stretching	Alkanes
2924.35	16214.60	C–H	Stretching	Alkanes or Alkyl groups
3417.53	19101.95	O–H	Stretching	Hydroxyl groups
3602.10	2459.01	O–H	Stretching	Free Hydroxyl groups

3.1.2. Ultraviolet and Visible Spectrophotometry of Chitosan

Figure 4 presents the UV–Vis absorption spectrum of the extracted chitosan sample, measured across a wavelength range of 200 to 700 nm. The absorbance values range from approximately 1.3 at 200 nm to 0.2 at 700 nm, forming a smooth, downward-sloping curve. The key observation is that the spectrum shows a strong absorbance peak in the 200–230 nm range, which is characteristic of π–π* electronic transitions. These transitions are typically associated with chromophore groups such as carbonyl (C=O) or conjugated double bonds, which may be present due to residual acetyl groups or minor impurities in the chitosan

structure. Beyond 300 nm, the absorbance gradually declines, and by 700 nm, it approaches a baseline level of ~0.2, indicating minimal absorption in the visible region. This implies that the high absorbance in the UV region confirms the presence of functional groups such as carbonyls, amines, and hydroxyls, which are typical in chitosan and its derivatives. The lack of significant absorbance in the visible range (400–700 nm) suggests that the chitosan sample is optically transparent in this region, which is desirable for applications in biomedical films, coatings, and packaging. The smooth decline in absorbance also indicates that the sample is relatively pure, with no strong visible-light-absorbing impurities. Previous studies by González-Martínez et al. [29] showed that chitosan typically exhibits a strong UV absorbance peak around 210–230 nm due to π–π* transitions in carbonyl-containing groups. Meynaud et al. [30] also reported that chitosan and its derivatives show minimal absorbance beyond 300 nm, confirming the trend observed in your sample.

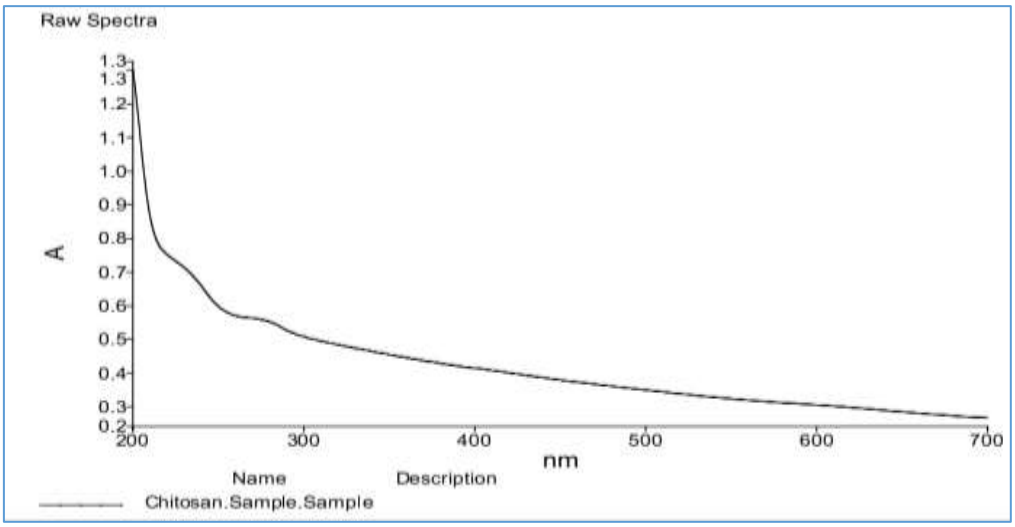

Figure 4. UV spectroscopy of chitosan

3.2. Experimental data

3.2.1. Effect of initial cadmium ion concentration

Figure 5 shows the relationship between the initial concentration of cadmium ions (Cd^{2+}) in solution and the percentage removal efficiency by citric acid-modified chitosan. The initial concentrations tested ranged from approximately 2 to 10 ppm. The removal efficiency was highest (91%) at 2 ppm, indicating that the number of available adsorption sites on the chitosan surface was sufficient to capture nearly all Cd^{2+} ions. As the concentration increased to 3 ppm, a sharp decline in removal efficiency to 85% was observed. This suggests that the number of cadmium ions began to exceed the number of available active sites, leading to competitive adsorption. Beyond this point, from 5 ppm to 10 ppm, the removal efficiency reaches equilibrium around 84–85%, indicating that the adsorbent surface was approaching saturation. The data implies that at low concentrations, the driving force for mass transfer is high, and the adsorbent surface is largely unoccupied, resulting in high removal efficiency. At higher concentrations, the adsorption sites become saturated, and the removal efficiency levels off despite the increase in available metal ions [14]. Similar trends were reported by Abbasi and Yousefi. [31] observed that chitosan-MWCNT nanocomposites showed high removal efficiency at low Cd^{2+} concentrations, with a decline and plateau at higher concentrations due to site saturation. Brandes et al. [32], using phosphorylated chitosan-cellulose composites, also reported a high removal efficiency beyond 10 ppm, consistent with monolayer adsorption behavior.

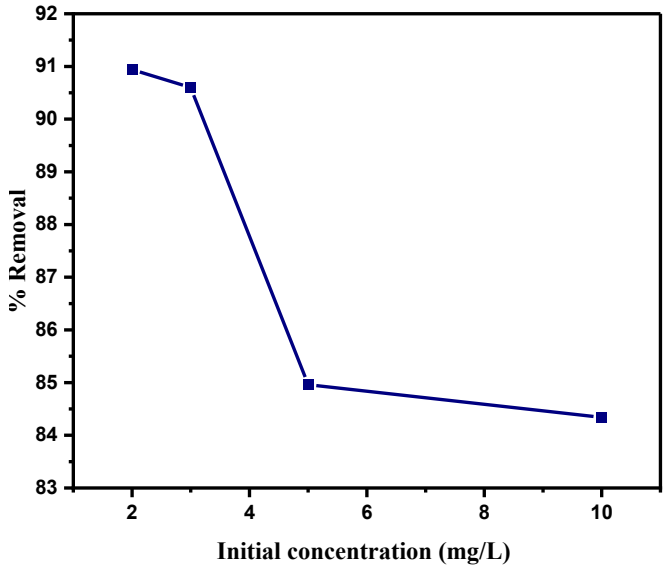

Figure 5. Effect of initial concentration

3.2.2. Effect of contact time on adsorption capacity

Figure 6 shows the effect of different contact time between cadmium ions (Cd^{2+}) and citric acid-modified chitosan. The rapid initial uptake shows that from 0 to 60 minutes; the adsorption capacity increases sharply. This indicates that the adsorbent surface has abundant active sites available for cadmium ion binding during the early stages of contact. At equilibrium, the data flattens, showing equilibrium has been achieved, thus desorption equals desorption. The initial phase is dominated by external surface adsorption, where cadmium ions rapidly bind to available functional groups (–NH_2, –OH, –COOH) on the chitosan surface [33]. As time progresses, intraparticle diffusion becomes the limiting step, and fewer active sites remain unoccupied. Abbasi and Yousefi [31] reported similar equilibrium behavior for chitosan-MWCNT composites, with equilibrium reached within 60 minutes and maximum adsorption capacity observed at that point. Brandes et al. [32] found that phosphorylated chitosan nanocomposites also reached equilibrium within 60–90 minutes, depending on temperature and pH.

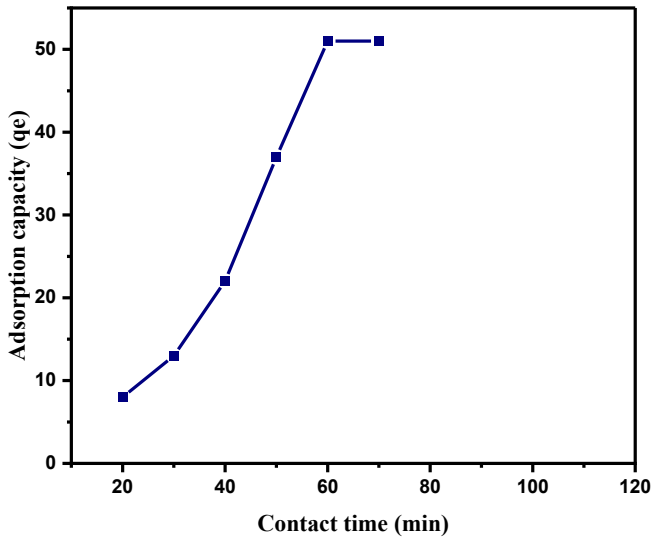

Figure 6. Effect of contact time

3.2.3. Effect of temperature on adsorption capacity

Figure 7 shows the effect of temperature on the adsorption capacity (q_e) of citric acid-modified chitosan for cadmium ion (Cd^{2+}) removal from aqueous solution. It was observed that at 40°C, the adsorption capacity is highest (96 %). As the temperature increases to 60°C, 80°C, and finally 100°C, the adsorption capacity decreases progressively, reaching a minimum of 20 units at 100°C. The trend is consistently downward, indicating an exothermic nature and a negative correlation between temperature and adsorption capacity. At lower temperatures, the interaction between Cd^{2+} ions and the functional groups (–NH_2, –OH, –COOH) on the chitosan surface is stronger, leading to higher adsorption [34]. As temperature increases, the kinetic energy of cadmium ions increases, which may disrupt the adsorbent–adsorbate interactions, cause desorption of previously adsorbed ions and alter the structure of the adsorbent, reducing the number of active sites [35]. Abbasi and Yousefi [31] reported a similar decrease in adsorption capacity with increasing temperature for chitosan-based nanocomposites, confirming the exothermic nature of Cd^{2+} adsorption. In contrast, Brandes et al. [32] observed endothermic behavior for phosphorylated chitosan-cellulose composites, where adsorption increased with temperature due to enhanced diffusion and activation of binding sites.

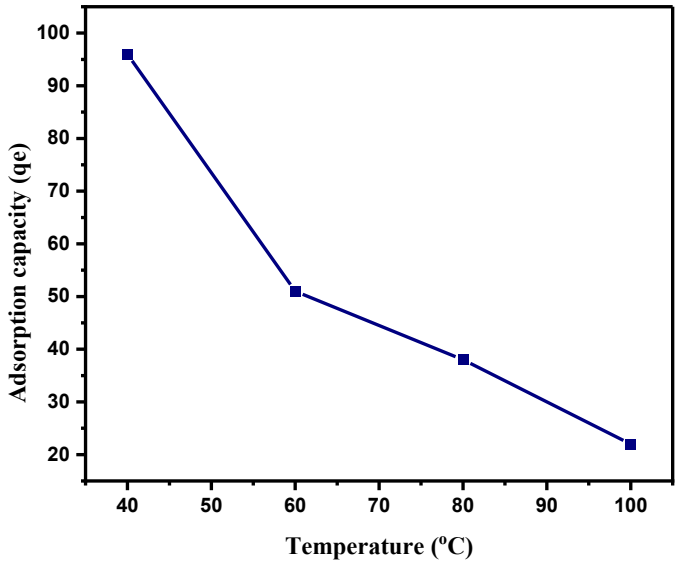

Figure 7. Effect of temperature

3.3. Adsorption Isotherm

Figure 8 and Table 3 show the Langmuir isotherm model plot, which is a linearized form of the Langmuir equation. q_{max} was 49.26mg/g, which is the theoretical maximum adsorption capacity of the modified chitosan. It represents the amount of cadmium that can be adsorbed per gram of adsorbent when all active sites are occupied. K_L (0.141 L/mg) is the Langmuir constant, which reflects the affinity between the adsorbent and the adsorbate. A higher value indicates stronger binding. In this case, the value is moderate, suggesting a reasonable interaction strength. The coefficient of determination, $R^2 = 0.0245$ value implies that the adsorption of cadmium onto modified chitosan does not follow Langmuir behaviour, which assumes monolayer adsorption on a homogeneous surface. This could be due to surface heterogeneity of the modified chitosan, multilayer adsorption or interactions between adsorbed species and incomplete saturation of adsorption sites [36, 37].

Figure 9 and **Table 3** depict the Freundlich isotherm model plot, which is a linearized form of the Freundlich equation. K_F indicates the adsorption capacity of the adsorbent (6.072), as a higher value reflects

a greater ability of the modified chitosan to adsorb cadmium ions. n (1.163) reflects the adsorption intensity and surface heterogeneity, as such since n > 1, this suggests favorable adsorption and a relatively homogeneous surface. R^2 (0.8389) indicates a moderate to good fit of the experimental data to the Freundlich model, which is significantly better than the Langmuir model (R^2 = 0.0245), suggesting that the adsorption occurs on a heterogeneous surface with multilayer formation [38].

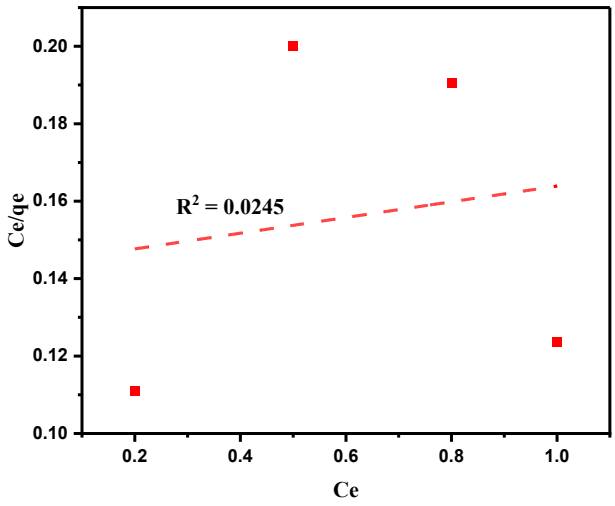

Figure 8. Langmuir isotherm plot

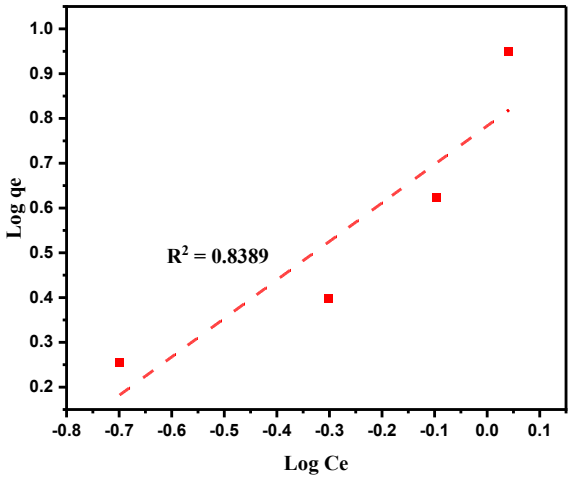

Figure 9. Freundlich isotherm plot

Table 3. Adsorption isotherm parameters

parameters	Langmuir
q_m(mg/g)	49.26
R^2	0.0245
K_L(L/mg)	0.141
	Freundlich
K_F(L/g)	6.072
n	1.163
R^2	0.8389

3.4. Kinetics Isotherm

The kinetics studies were evaluated using two widely accepted models, the pseudo-first-order and pseudo-second-order kinetic models. These models help to understand the rate and mechanism of the adsorption process. The pseudo-first-order model assumes that the rate of occupation of adsorption sites is proportional to the number of unoccupied sites. In Figure 10 and Table 4 (pseudo-first-order plot), the experimental equilibrium adsorption capacity ($q_{e,exp}$) was found to be 51 mg/g, while the calculated value ($q_{e,cal}$) from the model was 101.92 mg/g. The rate constant (k_1) was determined to be 0.036 min^{-1}, and the coefficient of determination (R^2) was 0.8730. Although the R^2 value indicates a moderate correlation, the large discrepancy between the experimental and calculated (q_e) values suggests that the pseudo-first-order model does not accurately describe the adsorption kinetics in this case [39].

The pseudo-second-order model, on the other hand, assumes that the adsorption process is governed by chemisorption, involving valence forces through sharing or exchange of electrons between the adsorbent and the adsorbate. From the experimental plot (Figure 11 and Table 4), the pseudo-second-order model yielded a rate constant (k_2) of 0.0004 g/mg·min and a calculated (q_e) of –27.54 mg/g. Despite the non-physical negative value of (q_e), the model showed a very high R^2 value of 0.9738, indicating an excellent fit to the experimental data. This strong correlation suggests that the adsorption process is better described by the pseudo-second-order model, supporting the hypothesis that chemisorption is the dominant mechanism [40]. The negative qe value obtained from the pseudo-second-order model, despite a high R^2, indicates a potential limitation in the linearization method. This anomaly suggests that non-linear kinetic modeling may provide a more accurate representation of the adsorption mechanism and should be explored in subsequent studies.

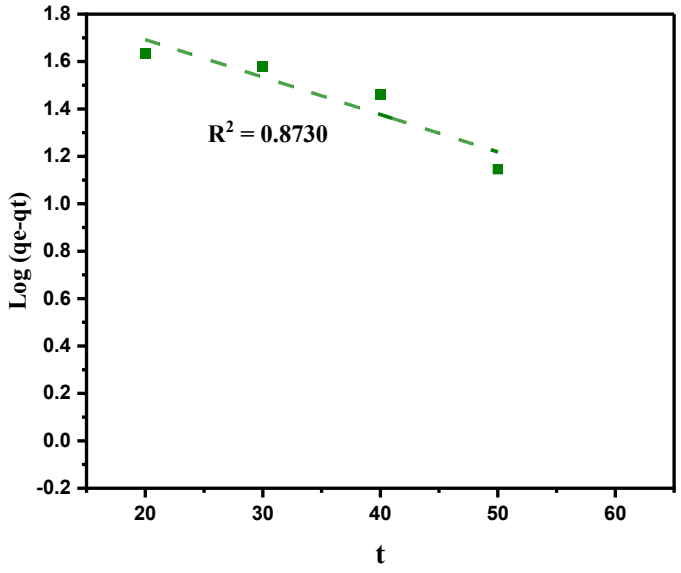

Figure 10. Pseudo-first order

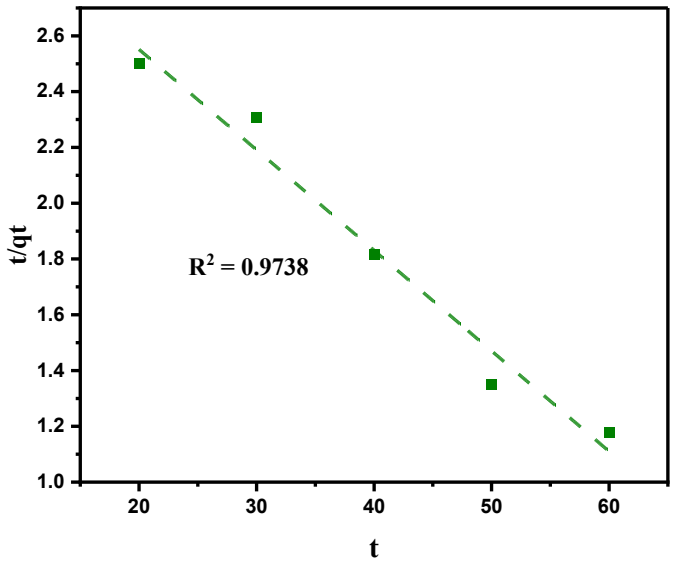

Figure 11. pseudo-second order

Table 4. Kinetics Isotherm data

parameters	**Pseudo first order**
qe_{exp} (mg/g)	51
k_1 (min^{-1})	0.036
qe_{cal} (mg/g)	101.92
R^2	0.8730
	Pseudo-second order
k_2 (mg/g.min)	0.0004
qe_{cal} (mg/g)	-27.54
R^2	0.9738

Conclusion

The comprehensive characterization and experimental evaluation of citric acid-modified chitosan derived from oyster shells have demonstrated its potential as an effective biosorbent for cadmium ion removal from aqueous solutions. The FTIR analysis confirmed the successful transformation of raw oyster shell material into chitosan through the disappearance of peaks associated with nitrile and thiol groups and the emergence of prominent hydroxyl and carbonyl bands. These functional groups are essential for cadmium ion chelation, providing the necessary active sites for adsorption. The UV–Vis. Spectroscopy further validated the structural integrity and purity of the extracted chitosan. The strong absorbance in the UV region (200–230 nm) and the absence of significant absorption in the visible range confirmed the presence of chromophoric groups and the optical clarity of the material, making it suitable for applications requiring biocompatibility and transparency. Experimental studies revealed that the modified chitosan exhibited high adsorption efficiency at low cadmium concentrations, with over 90% removal at 2 ppm. However, as the concentration increased, efficiency plateaued, indicating the need for higher adsorbent dosages or multi-stage treatment at elevated contaminant levels. The optimal contact time was determined to be 60 minutes, beyond which no significant increase in adsorption was observed. This equilibrium behavior aligns with the pseudo-second-order kinetic model, suggesting that chemisorption is the dominant mechanism governing the

adsorption process. Temperature studies indicated that cadmium adsorption is exothermic, with higher adsorption capacities observed at lower temperatures. This finding has practical implications for wastewater treatment, as it supports the use of ambient or slightly elevated temperatures to maximize efficiency while minimizing energy input. Isotherm modelling showed that the Langmuir model, despite predicting a high theoretical maximum adsorption capacity (Q_m = 49.26 mg/g), did not fit the experimental data well (R^2 = 0.0245), indicating that monolayer adsorption on a homogeneous surface is not the dominant mechanism. In contrast, the Freundlich isotherm provided a better fit (R^2 = 0.8389), suggesting that cadmium adsorption occurs on a heterogeneous surface with varying binding site affinities, consistent with the structural complexity introduced by citric acid modification. Kinetic modeling reinforced these findings, with the pseudo-second-order model yielding a higher correlation coefficient (R^2 = 0.9738) compared to the pseudo-first-order model (R^2 = 0.8730). Although the calculated equilibrium adsorption capacity in the second-order model was negative, likely due to linearization plots, the overall fit supports the conclusion that chemical interactions, rather than simple physical adsorption, play a significant role in cadmium uptake. In summary, the study confirms that citric acid-modified chitosan is a promising, low-cost, and environmentally friendly adsorbent for cadmium removal from wastewater. Surface heterogeneity, chemisorption mechanisms, and optimal operational parameters such as contact time and temperature govern its performance. Further optimization through nonlinear modelling and real-world wastewater testing is recommended to enhance its practical applicability. Future studies should explore non-linear modeling approaches and alternative isotherm models such as Temkin or Dubinin–Radushkevich to better capture the adsorption behavior. Validation using real industrial wastewater is also recommended to assess the adsorbent's performance under complex environmental conditions.

Conflict of interest

The authors declare no conflict of interest.

References

1. Genchi, G., Sinicropi, M. S., Lauria, G., Carocci, A., & Catalano, A. (2020). The effects of cadmium toxicity. International journal of environmental research and public health, 17(11), 3782. https://doi.org/10.3390/ijerph17113782
2. Charkiewicz, A. E., Omeljaniuk, W. J., Nowak, K., Garley, M., & Nikliński, J. (2023). Cadmium toxicity and health effects—a brief summary. Molecules, 28(18), 6620. https://doi.org/10.3390/molecules28186620
3. Burk, G. A., Herath, A., Crisler, G. B., Bridges, D., Patel, S., Pittman Jr, C. U., & Mlsna, T. (2020). Cadmium and copper removal from aqueous solutions using chitosan-coated gasifier biochar. Frontiers in Environmental Science, 8, 541203. https://doi.org/10.3389/fenvs.2020.541203
4. Selvi, A., Rajasekar, A., Theerthagiri, J., Ananthaselvam, A., Sathishkumar, K., Madhavan, J., & Rahman, P. K. (2019). Integrated remediation processes toward heavy metal removal/recovery from various environments-a review. Frontiers in Environmental Science, 7, 66. https://doi.org/10.3389/fenvs.2019.00066
5. Iber, B. T., Kasan, N. A., Torsabo, D., & Omuwa, J. W. (2022). A review of various sources of chitin and chitosan in nature. Journal of Renewable Materials, 10(4), 1097-1123. https://doi.org/10.32604/JRM.2022.018142
6. Gamage, A., Jayasinghe, N., Thiviya, P., Wasana, M. D., Merah, O., Madhujith, T., & Koduru, J. R. (2023). Recent application prospects of chitosan-based composites for the metal contaminated wastewater treatment. Polymers, 15(6), 1453. https://doi.org/10.3390/polym15061453

7. Wang, P., Li, L., Pang, X., Zhang, Y., Zhang, Y., Dong, W. F., & Yan, R. (2021). Chitosan-based carbon nanoparticles as a heavy metal indicator and for wastewater treatment. RSC Advances, 11(20), 12015-12021. http://doi.org/10.1039/d1ra00692d
8. Tsauria, Q. D., Gareso, P. L., & Tahir, D. (2025). Systematic review of chitosan-based adsorbents for heavy metal and dye remediation. Integrated Environmental Assessment and Management, vjaf037. https://doi.org/10.1093/inteam/vjaf037
9. Alshahrani, A., Alharbi, A., Alnasser, S., Almihdar, M., Alsuhybani, M., & AlOtaibi, B. (2021). Enhanced heavy metals removal by a novel carbon nanotubes buckypaper membrane containing a mixture of two biopolymers: Chitosan and ι-carrageenan. Separation and Purification Technology, 276, 119300. https://doi.org/10.1016/j.seppur.2021.119300
10. Rahman, A. (2024). Promising and environmentally friendly removal of copper, zinc, cadmium, and lead from wastewater using modified shrimp-based chitosan. Water, 16(1), 184. https://doi.org/10.3390/w16010184
11. Mola Ali Abasiyan, S., Dashbolaghi, F., & Mahdavinia, G. R. (2019). Chitosan cross-linked with κ-carrageenan to remove cadmium from water and soil systems. Environmental Science and Pollution Research, 26(25), 26254-26264. https://doi.org/10.1007/s11356-019-05488-1
12. Ohto, K., Ohta, S., Huang, K., Kawakita, H., & Inoue, K. (2017). Adsorption Behaviour of Dithiocarbamate β-Chitosan Gels for Cadmium (II). Research & Reviews: Journal of Material Sciences. 5(3): 1-9. http://doi.org/10.4172/2321-6212.1000175
13. Olaosebikan, A. O., Kehinde, O. A., Tolulase, O. A., & Victor, E. B. (2021). Extraction and characterization of chitin and chitosan from Callinectes amnicola and Penaeus notialis shell wastes. Journal of Chemical Engineering and Materials Science, 12(1), 1–30. https://doi.org/10.5897/jcems2020.0353
14. Kuczajowska-Zadrożna, M., Filipkowska, U., & Jóźwiak, T. (2020). Adsorption of Cu (II) and Cd (II) from aqueous solutions by chitosan immobilized in alginate beads. Journal of Environmental Chemical Engineering, 8(4), 103878. https://doi.org/10.1016/j.jece.2020.103878
15. Wang, X., He, M., Wang, X., Liu, S., Luo, L., Zeng, Q., ... & Jia, R. (2024). Emerging Nanochitosan for Sustainable Agriculture. International Journal of Molecular Sciences, 25(22), 12261. https://doi.org/10.3390/ijms252212261
16. Purohit, G., & Rawat, D. S. (2022). Characterization techniques for chitosan and its based nanocomposites. In: Gulati, S. (eds) Chitosan-Based Nanocomposite Materials: Fabrication, Characterization and Biomedical Applications. Springer, Singapore. 79-101. https://doi.org/10.1007/978-981-19-5338-5_3
17. Van der Horst, C., Silwana, B., Makombe, M., Iwuoha, E., & Somerset, V. (2021). Application of a chitosan bimetallic nanocomposite for the simultaneous removal of cadmium, nickel, and lead from aqueous solution. Desalination and Water Treatment, 220, 168-181. https://doi.org/10.5004/dwt.2021.26919
18. Omokpariola, D. O., & Otuosorochi, J. N. (2020). Adsorption of Congo red dye using Rice husk. World Scientific News, (150), 22-38.
19. Omokpariola, D. O., & Otuosorochi, J. N. (2021). Batch Adsorption Studies on Rice Husk with Methyl Violet Dye. World News of Natural Sciences, 33, 48-63.
20. Sumaila, A., Ndamitso, M. M., Iyaka, Y. A., Abdulkareem, A. S., Tijani, J. O., & Idris, M. O. (2020). Extraction and characterization of chitosan from crab shells: Kinetic and thermodynamic studies of arsenic and copper adsorption from electroplating wastewater. Iraqi Journal of Science, 61(9), 2156–2171. https://doi.org/10.24996/ijs.2020.61.9.2
21. Li, J., Lin, G., Zhong, Z., Wang, Z., Wang, S., Fu, L., & Hu, T. (2024). A novel magnetic Ti-MOF/chitosan composite for efficient adsorption of Pb (II) from aqueous solutions: Synthesis and investigation. International Journal of Biological Macromolecules, 258, 129170. https://doi.org/10.1016/j.ijbiomac.2023.129170

22. Adebisi, E. U., Adebisi, A. A., Okechukwu, V. U., Omokpariola, D. O., & Umeh, T. C. (2022). Adsorption potential of Lead and Nickel ions by Chrysophyllum albidum G. Don (African Star Apple) seed shells. World Scientific News, 166, 132-145.
23. Omokpariola, D. O. (2021). Experimental Modelling Studies on the removal of crystal violet, methylene blue and malachite green dyes using Theobroma cacao (Cocoa Pod Powder). Journal of Chemistry Letters, 2(1), 9-24. https://doi.org/10.22034/jchemlett.2021.272842.1020
24. Rasheed, R. M., Moghal, A. A. B., Jannepally, S. S. R., Rehman, A. U., & Chittoori, B. C. (2023). Shrinkage and consolidation characteristics of chitosan-amended soft soil—A sustainable alternate landfill liner material. Buildings, 13(9), 2230. https://doi.org/10.3390/buildings13092230
25. Ullah, S., Hayat, K., & Qiao, X. (2023). Chitosan-based biostimulation: A novel approach for simultaneous remediation of co-existing cadmium and arsenic contamination in soil. Air, Soil and Water Research, 16, 11786221231216862. https://doi.org/10.1177/11786221231216862
26. Yasin, M. U., Haider, Z., Munir, R., Zulfiqar, U., Rehman, M., Javaid, M. H., ... & Gan, Y. (2024). The synergistic potential of biochar and nanoparticles in phytoremediation and enhancing cadmium tolerance in plants. Chemosphere, 141672. https://doi.org/10.1016/j.chemosphere.2024.141672
27. Pandey, M., Mishra, S. M., Tiwari, A., Tirkey, A., Tiwari, A., Dubey, R., ... & Pandey, S. K. (2024). A systematic study on the synergistic effect of biochar-compost in improving soil function and reducing cadmium toxicity in Spinacia oleracea L. Environmental Technology & Innovation, 36, 103775. https://doi.org/10.1016/j.eti.2024.103775
28. Lalit Mahatma, N. A. M. (2021). Extraction and Characterization of Chitosan by Simple Technique from Mud Crabs. International Journal of Current Microbiology and Applied Sciences, 10(6), 513–518. https://doi.org/10.20546/ijcmas.2021.1006.055
29. González-Martínez, J. R., Magallanes-Vallejo, A. G., López-Oyama, A. B., Madera-Santana, T. J., Anaya-Garza, K., Rodríguez-González, E., ... & Gámez-Corrales, R. (2023). Improved mechanical, optical, and electrical properties of chitosan films with the synergistic reinforcing effect of carbon nanotubes and reduced graphene oxide for potential optoelectronic applications. https://doi.org/10.21203/rs.3.rs-2725043/v1
30. Meynaud, S., Huet, G., Brulé, D., Gardrat, C., Poinssot, B., & Coma, V. (2023). Impact of UV Irradiation on the Chitosan Bioactivity for Biopesticide Applications. Molecules, 28(13). https://doi.org/10.3390/molecules28134954
31. Abbasi, M., & Yousefi, R. (2016). Preparation, characterization and biosorption properties of chitosan-mwcnts nanocomposite for removal of cadmium from aqueous solution. Applied Chemistry Today, 10(37), 87-100.
32. Brandes, R., Brouillette, F. & Chabot, B. (2020) Laboratory Adsorption Studies on Cadmium (II) by Nonwoven Chitosan/Phosphorylated Microcellulose Nanocomposite. Water Air Soil Pollut 231, 566. https://doi.org/10.1007/s11270-020-04936-w
33. Umeh, T. C., Nduka, J. K., & Akpomie, K. G. (2021). Kinetics and isotherm modeling of Pb (II) and Cd (II) sequestration from polluted water onto tropical ultisol obtained from Enugu Nigeria. Applied Water Science, 11, 65. https://doi.org/10.1007/s13201-021-01402-8
34. Umeh, C., Asegbeloyin, J. N., Akpomie, K. G., Oyeka, E. E., & Ochonogor, A. E. (2020). Adsorption properties of tropical soils from Awka North, Anambra Nigeria for lead and cadmium ions from aqueous media. Chemistry Africa, 3, 199-210. https://doi.org/10.1007/s42250-019-00109-3
35. Umeh, C. T., Nduka, J. K., Mogale, R., Akpomie, K. G., & Okoye, N. H. (2024). Acid-activated corn silk as a promising phytosorbent for uptake of Malachite green and Cd (II) ion from simulated wastewater: equilibrium, kinetic and thermodynamic studies. International Journal of Phytoremediation, 26(10), 1593-1610. https://doi.org/10.1080/15226514.2024.2339478

36. Umeh, C.T., Nduka, J.K., Iwuozor, O.K., Omokpariola, O. D., Dulta, K., Ezeh, S. C., & Emeka, R. N. (2023). Adsorption modelling on the removal of ciprofloxacin antibiotic from aqueous solution by acid-modified corn cob. International Journal of Environmental Analytical Chemistry, 105(2), 432-457. https://doi.org/10.1080/03067319.2023.2263383
37. Umeh, C. T., Nduka, J. K., Akpomie, K. G., Ighalo, J. O., & Mogale, R. (2025). Adsorptive Effect of Corn Silk-Loaded Nickel Oxide and Copper Oxide Nanoparticles for Elimination of Ciprofloxacin from Wastewater. ACS omega, 10(4): 3784–3800. https://doi.org/10.1021/acsomega.4c09192
38. Et-Tanteny, R., Allaoui, I., Manssouri, I., El Amrani, B., & Draoui, K. (2025). Kinetic and isotherm studies of nickel and cadmium ions adsorption onto Clay-Chitosan composite. Results in Chemistry, 102056. https://doi.org/10.1016/j.rechem.2025.102056
39. Radha, E., Gomathi, T., Sudha, P. N., Latha, S., Ghfar, A. A., & Hossain, N. (2025). Adsorption studies on removal of Pb (II) and Cd (II) ions using chitosan derived copoymeric blend. Biomass Conversion and Biorefinery, 15(2), 1847-1862. https://doi.org/10.1007/s13399-021-01918-8
40. Salih, S. S., Shihab, M. A., Mohammed, H. N., Kadhom, M., Albayati, N., & Ghosh, T. K. (2024). Chitosan-vermiculite composite adsorbent: Preparation, characterization, and competitive adsorption of Cu (II) and Cd (II) ions. Journal of Water Process Engineering, 59, 105044. https://doi.org/10.1016/j.jwpe.2024.105044